University of New Mexico
UNM Digital Repository

Geography ETDs | Electronic Theses and Dissertations

Summer 7-30-2016

Modeling the Timeliness of Airborne Remote Sensing Data

Andrew Loerch

Follow this and additional works at: https://digitalrepository.unm.edu/geog_etds

 Part of the Environmental Sciences Commons

Recommended Citation
Loerch, Andrew. "Modeling the Timeliness of Airborne Remote Sensing Data." (2016). https://digitalrepository.unm.edu/geog_etds/31

This Thesis is brought to you for free and open access by the Electronic Theses and Dissertations at UNM Digital Repository. It has been accepted for inclusion in Geography ETDs by an authorized administrator of UNM Digital Repository. For more information, please contact disc@unm.edu.

Andrew C. Loerch
Candidate

Geography and Environmental Studies
Department

This thesis is approved, and it is acceptable in quality and form for publication:

Approved by the Thesis Committee:

Dr. Christopher Lippitt , Chairperson

Dr. Caitlin Lippitt

Dr. Danqinq Xiao

MODELING THE TIMELINESS OF AIRBORNE REMOTE SENSING DATA

by

ANDREW C. LOERCH

B.S., GEOGRAPHY, UNIVERSITY OF NEW MEXICO, 2014
B.A., GERMAN, UNIVERSITY OF NEW MEXICO, 2014

THESIS

Submitted in Partial Fulfillment of the
Requirements for the Degree of

Master of Science

Geography

The University of New Mexico
Albuquerque, New Mexico

December 2016

MODELING THE TIMELINESS OF AIRBORNE REMOTE SENSING DATA

by

ANDREW C. LOERCH

B.S., GEOGRAPHY, UNIVERSITY OF NEW MEXICO, 2014
B.A., GERMAN, UNIVERSITY OF NEW MEXICO, 2014
M.S., GEOGRAPHY, UNIVERSITY OF NEW MEXICO, 2016

ABSTRACT

The model, "Remote Sensing Communication Model" (RSCM), which permits the estimation of the timeliness of remote sensing systems (RSS) is tested (Lippitt, Stow, & Clarke, 2014). This model conceptualizes RSS as having capacities that determine the timeliness of the systems, where a system is comprised of three segments, each with a capacity that determines the timeliness of that segment: acquisition capacity, transmission capacity, and receiver capacity (i.e., the capacity of a human and/or machine analyst to produce information) (Lippitt et al., 2014). Acquisition and transmission capacity analyses are run to aid in the optimization of a flexible time-sensitive remote sensing system being designed for emergency response in Bernalillo County, NM. Modeled timeliness is validated using empirical tests of airborne acquisitions, the model modified to improve fit, and then used for a variety of manned and unmanned platform and sensor combinations to infer the timeliness of data delivery to emergency managers, based on both currently available and potential airborne assets. In doing so, this research assesses the accuracy of capacity based estimates of timeliness for airborne RSSs and demonstrate a method for the optimization of platform, sensor, and transmission configurations for emergency response.

Table of Contents

1. INTRODUCTION

Remote sensing is a critical hazard response technology and the timeliness of its information is critical for its effective use in hazard response (Bruzewicz, 2003; Cutter, 2003). Timeliness is defined by Lippitt as "the time between information request and the use of that information to inform a decision" (C. D. Lippitt, Stow, & Clarke, 2014). While we can predict the timeliness of image acquisitions from static systems with known temporal resolutions, such as satellites, it is far more difficult to predict the timeliness of acquisitions from aircraft and unmanned aerial systems. Predicting the timeliness of remote sensing systems prior to operational deployment is a requirement for time-sensitive remote sensing (Lippitt et al. 2014). When compared to satellites, aircraft acquisitions have additional factors affecting timeliness that makes it challenging to incorporate them into the standard operating procedures of emergency management organizations (C. Lippitt, Stow, & Coulter, 2015). The number of aircraft, their locations relative to areas at high risk for disasters, the types of aircraft, and the imaging sensors they operate, all affect the timeliness of data acquisition and delivery. As the literature review elucidates, accurately estimated timeliness of data delivery from airborne remote sensing systems is not currently incorporated into emergency managers' standard operating procedures, and this has resulted in limited use of remote sensing in response and recovery efforts (C. D. Lippitt et al., 2014).

This research tests a model called "Remote Sensing Communication Model" (RSCM), which permits the estimation of the timeliness of remote sensing systems (RSS) (Lippitt, Stow, & Clarke, 2014), for the estimation of timeliness for airborne RSSs. The

RSCM conceptualizes RSSs as having capacities that determine the timeliness of the systems, where a system is conceptualized as having three segments (sensor, channels, and receivers), each with a capacity that determines the timeliness of that segment based on the data volume to be acquired: acquisition capacity, transmission capacity, and receiver capacity (i.e., the capacity of a human and/or machine analyst to produce information) (Lippitt et al., 2014). To validate portions of the RSCM and to aid in the optimization of a flexible time-sensitive remote system being designed for emergency response in Bernalillo County, NM and San Diego County, CA this research performs and validates an acquisition and transmission capacity analysis. Modeled timeliness is validated using empirical tests of actual airborne acquisitions, the model is modified to improve fit, and used with a variety of extant platform and sensor combinations, operated by local aerial survey companies, to infer the timeliness of data delivery to emergency managers for six potential critical infrastructure sites based upon both currently available and potential manned and unmanned airborne assets. This research therefore assesses the accuracy of capacity based estimates of timeliness for airborne RSSs and demonstrates a method for the on demand optimization of platform, sensor, and transmission configuration for emergency response. The questions, "How accurately can the timeliness of airborne data acquisition and delivery be estimated, using the Remote Sensing Communication Model Capacity Analysis?", "Using RSCM Capacity Analysis, what is the estimated data delivery timeliness of extant aerial survey firms in support of a remote sensing system for hazard response in New Mexico and San Diego County, CA?", and "How will the introduction of UAS affect data delivery timeliness?" are answered in this thesis.

2. BACKGROUND

Before, during, and after a hazard event, there is an obvious desire to have and utilize best available information in an effort to prevent damage to property and loss of life. Emergency managers and disaster responders have previously used combinations of on the ground assessments, satellite imagery, and airborne imagery, to collect this information, with varying degrees of success (Cutter, 2003; Ehrlich, Guo, Molch, Ma, & Pesaresi, 2009).

Disasters and hazards can be local, regional, and global in their effects on places and people. Often, there is little time to prepare for an impending disaster, and once such an event occurs, there is often a short window of hours-days available in which to rescue survivors and assess damaged critical infrastructure (Cutter, 2003; C. Lippitt et al., 2015). For these reasons, the types of technologies and information necessary for improving disaster prevention and response across spatial and temporal scales continues to be an active research area. This review looks at how emergency managers utilize remotely sensed data, models for estimating the acquisition and delivery timeliness of imagery, and the potential benefits of small unmanned airborne systems (S-UAS) to image acquisition and delivery timeliness.

2.1 The Disaster Management Framework and User Needs

Determining the data needs of emergency managers and disaster responders first requires an understanding of the types of groups that provide disaster management, the frameworks in which they operate, and how they use various types of remotely sensed data.

Modern disaster management regimes exist at scales that range from neighborhood communities and local governments, up to national and global levels. These regimes also consist of formal and informal institutions (Cutter, 2003). Formal institutions are generally governmental agencies and well-established non-profit organizations, and informal institutions can be individuals, volunteer groups, impromptu aid and donation organizations and funds, the media, etc. Often, disaster management involves coordination between these agencies and networks to share financial, technological, and personnel resources, as well as information.

Most formal disaster management institutions, which are the primary focus of this research, recognize and use a structured framework called the "Disaster Management Cycle" (Gitas, Polychronaki, Katagis, & Mallinis, 2008; Laben, 2002). This cycle, which is also referenced in the majority of literature reviewed in this thesis, consists of phases. The pre-disaster and inter-disaster phases are: Reconstruction, Mitigation, and Preparedness. The post-disaster phases are: Rescue, Relief, and Recovery. These six phases are often condensed as Mitigation, preparedness, response, and recovery (Laben, 2002). It is helpful to think of disaster and hazard management in these phases as most remote sensing technologies have varying degrees of usefulness depending on the phase. The current trend shows that satellite and airborne remote sensing systems are being adopted heavily for Reconstruction, Mitigation, Preparedness and Recovery, but not in the Rescue and Relief phases (Cutter, 2003; Laben, 2002). The Reconstruction, Mitigation, Preparedness, and Recovery phases generally span longer time frames, which makes them more likely to be compatible with the slow acquisition, processing,

transmission, and publication times that are historically typical for remote sensing (Cutter, 2003; Joyce, Belliss, Samsonov, McNeill, & Glassey, 2009).

There remains significant interest in the potential for using satellite, manned, and unmanned remotely sensed data for the Rescue and Relief phases, but acquisition and processing times make supplying information within the first 48 hours challenging and, therefore, remote sensing derived information for hazard response unreliable (Bruzewicz, 2003). For these reasons, remote sensing derived information for Rescue and Relief still remains a largely supplementary, rather than primary, source of information. Ready estimation of data delivery timeliness could lead to increased use and usability of remote sensing in these two critical phases of the emergency management cycle (C. D. Lippitt et al., 2014). These gaps include a better understanding of the existing capacity of aerial survey firms to provide timely remote sensing data and an improved understanding of the accuracy of models used to estimate RSS information timeliness.

2.2 Remote Sensing Technologies for Disaster Response

The overall trend in disaster management has been an increase reliance upon remote sensing across the phases of the disaster management cycle (Colomina & Molina, 2014; Cutter, 2003; Laben, 2002; Metternicht, Hurni, & Gogu, 2005). Features depicted in imagery (e.g., structures, transportation infrastructure) taken before and after disaster events, are often classified based on degrees of damage from automated or manual change-detection (C. D. Lippitt & Stow, 2015).

Satellite and aircraft-based imagery have been useful in the preparedness, recovery and reconstruction phases of several disaster types, including: earthquakes, tsunami, hurricanes, landslides, and floods (Cutter, 2003; Eguchi & Huyck, 2001; Ehrlich et al.,

2009; Jeyaseelan, 2003; Joyce, Belliss, Samsonov, McNeill, & Glassey, 2009; Laben, 2002; Metternicht et al., 2005).

Specific applications of remote sensing to the hazard response phase include: evaluating the immediate aftermath of the Indian Ocean Tsunami 2010 via satellite imagery (Cutter, 2003; Laben, 2002; Laituri & Kodrich, 2008), a damage detection assessment using passive optical imagery and Synthetic Aperture Radar after the Marmara Earthquake of 1999 (Eguchi & Huyck, 2001), damage detection after the Wenchuan Earthquake of 2008 using high-resolution satellite imagery and Synthetic Aperture Radar (Ehrlich et al., 2009), the extent of fire damage and vegetation loss from the Peloponnese fires in 2007 using moderate-resolution satellite imagery (Gitas, Polychronaki, Katagis, & Mallinis, 2008), and the 2008 Super-Sauze Landslide using very high-resolution UAS-based imagery (Niethammer, James, Rothmund, Travelletti, & Joswig, 2012; Westoby, Brasington, Glasser, Hambrey, & Reynolds, 2012).

The data acquired from aircraft and satellites for these various disasters typically exhibit spatial resolutions of 0.05m to 0.25m for aerial, and between 1m – 1km for satellites (Ehrlich, Guo, Molch, Ma, & Pesaresi, 2009; Joyce et al., 2009; Metternicht, Hurni, & Gogu, 2005). Aerial and satellite imagery provide synoptic sampling over large spatial extents, and therefore make it possible to detect damage to critical infrastructure over large extents. Unfortunately, imagery could potentially be unavailable for an area for a significant (>72 hours) period of time if the weather conditions make flying impossible, if the area is covered in clouds or smoke, and if the timeliness of the acquisitions are uncertain or not accounted for in standard operating procedures (Cutter, 2003; Ehrlich et al., 2009; C. Lippitt et al., 2015). To minimize processing and analysis times and

improve trust in results, the disaster management community still primarily uses manual image interpretation and ground inspections of damaged areas for initial rescue and recovery operations (Joyce et al., 2009; C. Lippitt et al., 2015). Despite the trend of increased reliance on remote sensing data, delays in information delivery, a lack of reliability and certainty in the expected timeliness of the systems, and the lack of inclusion of the systems in standard operating procedures have made the systems less effective in the response and recovery phases of the DMC.

2.2.1 S-UAS for Hazard Response

Small Unmanned Aerial Systems (S-UAS) are currently being studied and in some cases used operationally for image acquisitions in order to address some of the problems related to timeliness of damage detection (Niethammer, James, Rothmund, Travelletti, & Joswig, 2012). Specifically, S-UAS are being used to monitor the Super-Sauze landslide progression because of their ability to be rapidly deployed and create digital surface models with ground sample resolutions of 0.03m to 0.08m (Niethammer et al., 2012).

S-UAS are capable of being deployed at lower-cost and with less technical training than manned aircraft or their larger unmanned counterparts, are capable of multi-spectral imaging, and their low-altitudes make them ideal for capturing data at hyper-spatial resolutions (Westoby et al., 2012; Zhang et al., 2015; Zhang, Lippitt, Bogus, Loerch, & Sturm, 2016). S-UAS acquired remote sensing for both rapid (within 24 hours) and real-time (imagery is processed and delivered as a disaster is occurring) hazard response improves upon the manned and satellite platform timeliness delays of up to 72 hours.. Following the Fukushima nuclear disaster, Tokai and Nihon universities in Japan began a project to demonstrate the capability of S-UAS based remote sensing in conjunction with

satellite imagery to provide continuous (daytime) data about the disaster (Baltsavias, Cho, Remondino, Soergel, & Wakabayashi, 2013).

Current U.S. Federal Aviation Administration classifications of UAS are based upon their total weight and maximum airspeed (Maddalon, Hayhurst, Morris, & Verstynen, 2013), whereas manufacturers and users of UAS typically rely on a classification system based upon the UAS' capabilities and characteristics (Watts, Ambrosia, & Hinkley, 2012). "Nano Aerial Vehicles", for example, are UAS that are the size of small birds and can be immediately launched in the event of a disaster, and "High Altitude, Long Endurance" or "HALE" systems are capable of flight durations of over 30 hours and can be launched within minutes of a disaster (Watts, Ambrosia, & Hinkley, 2012). The FAA classification of "Category 1 Small UAS" (S-UAS) consists of vehicles whose maximum weight including payload is 55 lbs or less with an airspeed less than or equal to 70 knots (Maddalon et al., 2013). Operators of this class of UAS are currently being granted exemptions to Section 333 of the FAAs rules governing commercial use of aircraft, making them legal for use under strict altitude and airspace conditions (George, 2015). These exemptions, coupled with the low-cost, off-the-shelf availability and hyper-spatial resolutions of S-UAS, make them ideal candidates for inclusion in the disaster management cycle and associated standard operating procedures of emergency managers.

As with traditional remote sensing platforms, most UAS carry sensors that are capable of imaging in some combination of visible and near-infrared wavelengths (Nebiker, Annen, Scherrer, & Oesch, 2008). This capability allows them to be used for vegetation and other multispectral indices that are useful for damage assessment and

management applications (Franke, Roberts, Halligan, & Menz, 2009; Lerma, Navarro, Cabrelles, & Villaverde, 2010; Roberts, 1999).

Small unmanned aerial systems generally require light-weight imaging sensors (Colomina & Molina, 2014), and the trend of cameras' resolutions increasing while simultaneously steadily decreasing in physical size and weight has meant that hyper-spatial ground resolutions can be achieved using consumer-off-the-shelf digital cameras. These systems, largely due to the altitudes at which they are safely flown, are capable of capturing images with resolutions in the millimeter range (Smith, Chandler, & Rose, 2009; Turner et al., 2003). The size and imaging sensor capabilities of these S-UAS systems are expected to result in their increased use for scientific research and infrastructure/emergency management (C. D. Lippitt, 2015).

It is clear from the literature that Unmanned Aerial Systems address the limitations of spatial resolution, rapid deployment, and cost associated with remote sensing as a disaster management tool. We therefore assess the timeliness of data delivery from S-UAS, as a likely near-term technology, to assess their potential impact on data delivery timeliness for hazard response.

2.3 Estimating the Timeliness Capacity of Remote Sensing Systems

Understanding the amount of time necessary to move any given imaging sensor and platform into place, acquire images, and deliver the imagery to analysts is both fundamental to the decision making process of which sensors and platforms to use, and the incorporation of remotely sensed imagery into the standard operating procedures of emergency managers (Joyce et al., 2009; C. Lippitt et al., 2015). The answer to the fundamental question, "How long will it take to receive useful information from remotely

sensed imagery during this disaster event" is one of the goals of information theory models intended to estimate timeliness (C. D. Lippitt et al., 2014; C. Lippitt et al., 2015).

The Remote Sensing Communication Model (RSCM) is a conceptual model of remote sensing based on information theory that was developed to inform the configuration of RSSs in the context of Time Sensitive Remote Sensing (TSRS) (C. D. Lippitt et al., 2014). The concept of modeling RSS capabilities dates back to the Strahler Remote Sensing Model (RSM) and subsequent derivatives (Phinn, 1998; Strahler, Woodcock, & Smith, 1986). While these models aided in the identification of appropriate data and analysis techniques for the extraction of a given information type, and some included a temporal component (Phinn, Stow, Franklin, Mertes, & Michaelsen, 2003), they did not address the question of timeliness in the configuration RSSs. The RSCM addresses this question by conceptualizing the process of obtaining information as having a source (i.e., reality of the scene to be imaged), an encoder of that reality (i.e., the sensor), a channel that communicates that encoded reality, and a receiver (analyst) that decodes that reality into information and delivers it to a user, each with a capacity that collectively determines the capacity of the RSS to transmit information from the source to users of that information (e.g., decision makers). See Figure 1 for a graphical depiction of the RSCM. These are identified as the Sensor Capacity, Transmission Capacity, and Analyst Capacity (C. D. Lippitt et al., 2014). Given any specifically configured imaging sensor, delivery platform, data transmission and analyst type, the timeliness of an RSS can be estimated based on these capacities. The result is an overall assessment of the timeliness of any given Remote Sensing System, and therefore the answer to the

question, “How long will it take to receive a given type of information from remotely sensed imagery during this disaster event?”.

2.3.1 Acquisition Capacity

Acquisition Capacity determines the timelines of acquisition, which is a product of the sensor and platform. Components of this segment of the RSCM include the size of the sensor’s imaging array, view angle (i.e., focal length), the altitude of the aircraft above ground, the number of flight lines, overlap, and distance flown to transition from one flight line to the next, etc. (C. D. Lippitt et al., 2014). In other words, sensor capacity reflects the amount of time required to move an aircraft and camera from the location where it is stored to the area to be imaged and acquire imagery.

The following equations and explanations for Acquisition Capacity are from Lippitt et al. 2014. Acquisition Capacity is given as:

$$\boldsymbol{T_{Acq} = \frac{B_S}{C_{Acq}} + T_D + T_M(N - 1)} \quad (1)$$

where T_D is the amount of time it would take the aircraft to reach the targeted region, T_M is the amount of time it takes to transition from one flight line to the next, and N is the number of flight lines required to cover the region. B_S is the “total number of bits required to image the scene,” and this is determined by the formula:

$$B_S = F\left(B_A A_S (1 + E_S)\right) \quad (2)$$

where F is the "compression factor" used by the imaging sensor, B_A is the bits per unit ground area, A_S is the total area of the targeted region, and E_S is the percentage of redundant acquisition due to necessary side lap and overlap. The bits per unit ground area, B_A, is estimated by:

$$B_A = \frac{B_P}{R_{G^2}} \quad (3)$$

where R_G is the ground sampling distance and B_P the number of bits required to store a pixel. The last variable of the time of acquisition formula, C_{Acq}, is estimated by:

$$C_{Acq} = \beta B_A \quad (4)$$

where β represents the rate of acquisition in area per unit time, given by:

$$\boldsymbol{\beta = D_W V} \quad (5)$$

where D_W represents the "swath width in ground distance" and V is the velocity of the aircraft.

2.3.2 Transmission Capacity

Transmission Capacity determines the timeliness of image delivery from the sensor to the analyst and from the analyst to the information user. This segment of the model accounts for the total amount of data acquired by the sensor(s) in bits and the expected

transmission rates of the sensor's hardware, the bandwidth of the specific networks used for transmission, any other potential transmission channels, and includes latencies that can be expected either with the chosen data transmission channels and with human interactions.. The following equations and explanations for Transmission Capacity are from Lippitt et al. 2014. The time required to transmit the data from the imaging sensor to the analyst, T_{Chan}, is estimated by:

$$T_{Chan} = \sum_{i}^{N} 1 \frac{B_S}{C_{Chan,i}} + L_i \quad (6)$$

Transmission channel segments, *i*, each need to be modeled individually. The variable C_{Chan} is the channel/transmission capacity in bits per unit time. The variable *L* represents latencies in data transmission that are related to medium limitations and human factors such as approval processes.

2.3.3 Analyst Capacity

Analyst Capacity determines the timeliness of generating and delivering actionable information in the forms of change detection maps, etc. Analyst timeliness is more easily estimated when the analyst is an automated process running on a computing system, stated as a function of the quantity of bits received from the imaging sensor, the complexity of processing, and the processing speed of the system, but can be estimated for manual (i.e., human) receivers as well. Because this research investigates only Sensor and Channel capacities, Analyst capacity analysis was excluded from the analysis.

This RSCM can be leveraged in a couple ways within the disaster management framework and the standard operating procedures of emergency managers, in order to

increase both the use and usability of remote sensing during the time-sensitive phases of disaster management (C. Lippitt et al., 2015). The RSCM could be used explicitly in the design and configuration of a system that satisfies the information needs of emergency managers, but can also be used to estimate the timeliness of flexible RSSs dynamically, in order to inform emergency managers which sensor/aircraft system to deploy for varied disaster scenarios.

The use of remote sensing for disaster management, and the number and types of people and organizations that are doing so, continues to increase. Newer technologies, such as flexible RSSs, requires the ability to accurately estimate the timeliness of data collection and delivery.

3. METHODS

The methods used in this research involved data collection from a number of sources, the creation of "Aerial Data Acquisition Processing Transmission - Timeliness Estimator" (ADAPTTE), a computer application implementation of the Remote Sensing Communication Model, and an analysis of data delivery timeliness for past and potential sensors and platforms. After implementation of the RSCM in ADAPTTE, initial model validation was performed using empirical flight records. Model validation by term was used to identify changes to the RSCM that improved model fit; these changes were implemented in ADAPTTE and timeliness for a matrix of aircraft and sensor combinations was modeled for the six critical infrastructure sites based upon extant aerial survey firms actual capacities and the hypothetical use of on-site or nearby S-UAS.

3.1 Data

The data collected and used in this research was derived from a survey of aerial imaging firms, manufacturers specifications, and actual image acquisition flights from manned and unmanned remote sensing systems.

3.1.1 Field Data

The Acquisition and Transmission Capacity components of the RSCM used in this analysis had not been rigorously tested, and therefore twelve actual flights were conducted and used to validate the model prior to its use for estimating data delivery timeliness for hazard response in Bernalillo County, NM. The data collection involved eight flights with two different manned aircraft and sensors, and four flights with a single unmanned aircraft equipped with two different sensors. The company Near Earth

Observation Systems provided the manned flights using a Quicksilver GT-500 ultralight aircraft with a Canon 5D Mark II sensor, and a Cessna with a Nikon D800. Regions imaged during the manned flights were: six flights at the Deer Creek Plateau, South of Albuquerque, NM (Figure 2), one flight over a portion of the Rio Grande River in Albuquerque, NM (Figure 3), and one flight over the San Diego State University (San Diego, CA) campus (Figure 4). The four unmanned aircraft flights were conducted using the 3D Robotics Iris+ Quadcopter and the SX260HS and Elph 130IS cameras. Regions imaged during the unmanned flights were: two flights near the North Domingo Baca Park in Northeast Albuquerque, NM (Figure 3), one flight near the University of New Mexico's North Campus golf course in Albuquerque, NM (Figure 5), and one flight at the Little Painted Desert, North of Winslow, AZ (Figure 6).

Information from the flights necessary to validate the Acquisition Capacity component was collected from a combination of specifications from the aircrafts' and sensors' makes/models, and the flight/sensor logs. These logs contain information about aircraft speed, velocity, flight path, and image station locations. Information necessary to validate the Transmission Capacity component was collected from the image data volume folder attributes, and transmission channel rates were based on IEEE and USB standards (Intel et al., 2000; Ramamurthy & Ashenayi, 2002; Seifert, 1998).

3.1.2 Survey Data

Answering the proposed research question required specific platform, sensor, and operating procedure data from individual aerial survey firms with the potential to service New Mexico and or San Diego County, CA. This data was acquired through an online survey of aerial survey firms in the Southwester United States. The firms were identified

through the Google Maps Database and the American Society of Photogrammetry and Remote Sensing's list of sustaining members and selected based upon their geographic locations: Southern California, Arizona, New Mexico, and Colorado.

Detailed questions were asked about each business, their aircraft, sensors, operating procedures, etc., in order to generate the numerical values necessary to satisfy the input variables of the RSCM Acquisition and Transmission Capacity model components. This allowed for estimation and ranking of each of aerial survey firms' platform/sensor combinations and transmission methods to provide timely data to emergency managers. Because some firms contract work to pilots and aircraft they do not employ or own, and because this could lead to redundant samples of aircraft/sensor combinations, an initial disqualifying question for the online survey was whether or not the responding firm owns and operates its own aircraft.

The Ubuntu Linux server that hosted the survey was located in the Geography department and used a static internet protocol address and domain name system. The web server software was Apache, with a Joomla content management front-end. The survey used a customized version of the Joomla extension "BF Survey." The entire site was accessed using secure socket layer encryption with a certificate purchased through The University of New Mexico's Information Technology Department, in order to ensure encrypted transmission of the survey data.

Of the original 70 Aerial Survey Firms identified as potential online survey participants, 44 were found to be ineligible. Criteria for ineligibility included: not owning/operating own aircraft, not performing aerial survey work, or the company no longer is in business. Of the remaining 26 eligible firms, eight responded, although two

of those responded that they operate only film-based systems and were therefore also excluded, leaving six usable survey responses. There were a total of 14 non-responses, with 5 being direct declines. The total response rate for the survey was 31% of identified eligible firms.

Of the six responses used in this research, three own and operate a total of four aircraft with multiple sensor options South of Los Angeles, California, one operates a single aircraft and sensor from the Phoenix Metro area of Arizona, one operates a single aircraft and sensor in New Mexico, and one operates an aircraft and sensor located in Kansas but expressed a willingness to fly surveys, "Anywhere West of the Mississippi." Information about the specific variables satisfied by the survey responses can be found in Table 1, and the extant aerial survey firms' platform/sensor combinations is in Table 2.

3.1.3 UAS Data

Performance specifications from two different S-UAS were used to model the timeliness of example S-UAS compared to traditional manned aircraft. Because of the demonstrated ability of S-UAS to operate in swarms (Daniel, Dusza, Lewandowski, Wietfeld, & De, 2009), this modeling included the hypothetical use of 1-3 individual S-UAS of a given model to cover an area.

The Iris+ Quadcopter developed by 3D Robotics and S1000+ Octocopter developed by DJI were used to represent Vertical Take-Off/Landing (VTOL) small unmanned aerial systems (S-UAS). The Iris+ carries a lightweight consumer of the shelf camera point and shoot camera, the Canon PowerShot SX260 while the DJI Spreading Wings S1000+ carries Nikon D810, a consumer digital single lens reflex full-frame camera with a 35mm lens. Specifications for these systems were gathered from the manufacturers and used in

the same manner as the survey data in order to create timeliness estimates of the case study regions, based upon these systems.

3.1.4 Targeted Regions/Sites

The targeted regions and sites in this section differ from those used for the model validations. Six sites were chosen from locations listed as "Critical Infrastructure Sites" by a separate survey of emergency managers that is ongoing as part of a National Science Foundation funded study on the optimization of remote sensing networks for monitoring critical infrastructure. From the list of critical infrastructure identified sites were selected to encompass a range of scene sizes. The San Vicente Dam and associated reservoir site, in Southern California, was chosen because it represents a potential critical infrastructure feature that is 182 hectares (Figure 7). The Del Mar Pump Station, in Southern California, was chosen because it represents a small area, 0.44 hectares, covering a single building and nearby concrete sewage-system enclosure (Figure 8). The North Torrey Pines Bridge, in Southern California, was chosen because it represents a potentially critical transportation infrastructure feature that covers an area of 3.1 hectares (Figure 9). The New Mexico South Capital Complex, in Northern New Mexico, was chosen because it is a relatively large area, 73.2 hectares, that encompasses several potentially critical state department buildings and road features (Figure 10). The Cochiti Lake, in Central New Mexico, was chosen because it is located in a remote area and encompasses 2,987 hectares (Figure 11). The Sandoval County Detention Center, in Central New Mexico, was chosen because, like the Del Mar Pump Station, it represents a smaller area of 14 hectares (Figure 12). The primary impetus for choosing the six sites is that they were

identified as “Critical Infrastructure” by emergency managers in the aforementioned ongoing survey of emergency managers.

3.2 Analysis

The program ADAPTTE was created using Equations 1-6 in Section 2.3.1 and Section 2.3.2. Using ADAPTTE with the field data collected from the flight logs and manufacturer specifications for the actual flights, the model was validated, revised based on evaluation of errors by term, and re-validated. The data collected from the aerial survey firms, and from the manufacturers’ specifications for the S-UAS platforms, was then used as inputs for the revised RSCM.

3.2.1 Implementation of the Model in Code

To facilitate practical and dynamic on-the-fly use of the RSCM, it was necessary to implement it in a computer application. Python was chosen as the scripting language most adaptable and suitable for the scope of this thesis, as it allows for the code to be utilized on a number of computing platforms, without complex development environments, and it could be readily ported to either a web application programming interface or an ESRI ArcGIS plugin. PostgreSQL was chosen as the database from which to read and write the model’s parameters and results.

ADAPTTE introduces a method for calculating T_m in the RSCM. T_m represents the transition time between flight lines, and is a function of the distance between flight lines. The RSCM, as written in Lippitt et al. 2014, accounts for, but does not specify, a specific mathematical method for calculating this term. Given the combination of physics, aircraft specifications, and human pilot interactions involved in transitioning between flight lines, implementing a reasonable definition for T_m is not trivial (Dashora & Lohani, 2013). The

definition implemented in ADAPTTE for T_m is based upon pseudo-code (Dashora & Lohani, 2013) for generating transition paths between flight lines using the flight line spacing, maximum bank angle of the aircraft, and velocity of the aircraft. ADAPTTE checks aircraft and scene parameters to determine whether a U-turn is suitable, whether an extended heading change and return curve to the following flight line is required, and then outputs a total transition time, T_{m}, based upon the above determinants. Because the VTOL UAS used in the field data was observed to perform 90° turns and pursue a straight path to the following flight line, an additional parameter not existing in Dashora 2013 was included to check for whether the aircraft used in the model is a VTOL UAS capable of performing direct path transitions.

3.2.2 Model Validation

There are two portions of the model that are validated in this paper: Acquisition Capacity and Transmission Capacity. In order to provide validation of acquisition and transmission capacity estimates, manned and unmanned aircraft and sensors were deployed for several flights each and the timeliness results compared to those predicted by the model. Percent Error and linear models reported as Adjusted R^2 are the metrics used for assessing how well the terms T_{Acq}, $B_{\mathrm{S}}/C_{\mathrm{Acq}}$, T_{M}, T_{D}, T_{Chann}, and B_{S} fit the actual flight results. An additional metric, Root Mean Squared Error, is used for assessing the overall error in T_{Acq} and T_{Chann}. These metrics are later used to provide an indication of the model's accuracy when predicting the acquisition and transmission timeliness of hypothetical flights.

For the Acquisition Timeliness validation assessment, the parameters listed in Table 1 were acquired for each aircraft, sensor, and region. The manned flights utilized an image

acquisition hardware/software system called “Aviatrix”. This system outputs many flight log files, three of which were used in every manned flight validation. The “PhotoCenters.txt” file provided timestamps of each image, making it possible to determine when a flight line began, when it ended, and when the next one began. The time elapsed between the end of one flight line and the beginning of another made it possible to determine the actual time spent transitioning between flight lines, T_m. These time stamps also made it possible to determine the actual time spent imaging the scene. The actual value of bits required to image the scene, Equation 10, was determined by converting the reported total file size of all images actually acquired during the flights from bytes to bits. The actual value of T_D, travel time to and from the scene, was derived from the first and last image timestamps in the “PhotoCenters.txt” file, and from the first and last GPS coordinates/heading timestamps in the “Trax.txt” files, which records the aircraft’s flight path in decimal degrees and heading, every ten seconds. The dimensions of the scenes that were imaged were derived from the “PhotoCenters.txt” files, with half the value of swath width covered by a line of images added to the boundary of the scenes.

The aircraft specifications, cruise velocity, maximum velocity, and maximum bank angle are added to a row in the database and used in part for calculating the times spent imaging, transitioning between flight lines, and moving to and from the scene. The aircraft platform’s associated sensor specifications, sensor width and height, image width and height, focal length, radiometric and spectral resolutions are then added and used in calculating the sensor capacity and data volume. Additional information regarding the sensor transmission channels were then added and used to assess transmission timeliness, T_{Chan}. The dimensions of the scene to be imaged are included, and in conjunction with the

aircraft and sensor specifications and a desired Ground Sample Distance, timeliness estimates are created using ADAPTTE. The values for all individual terms are also output by ADAPTTE.

Model validations for the four unmanned flights were performed identically to the manned flights as described above, with two exceptions. The autopilot hardware/software on the 3D Robotics Iris+ outputs a single log file containing all of the in-flight parameters, including those that contain the same values as Aviatrix; photo center coordinates and timestamps, and complete path of the UAS. Also, an aircraft platform parameter is set in ADAPTTE to indiciate the platform is a VTOL aircraft, thereby affecting how ADAPTTE calculates T_M. As was previously mentioned, T_M for VTOLs is calculated as a direct trajectory between flight lines rather than a curved path.

The assessment of transmission timeliness accuracy is performed using two sets of data for each of the eleven flights where the actual imagery was available. The first set of data comprised the actual imagery from each flight, and the second was the modeled data volumes from the Acquisition Capacity analysis. The SDSU Campus flight was excluded from the transmission analysis as the actual data was unavailable. In the context of this research, where the purpose of the model validation is to determine how well the RSCM can predict timelines compared to reality, it was not possible to know how long it actually took for the data to be delivered from the sensor to the analyst for the actual flights. Those times were not recorded during the initial data collection. Given that the actual flights were not originally conducted for time sensitive applications, the actual transmission times (T_{Chan}) would not be indicative of those we would expect under hazard response. The transmission capacity validation is therefore conducted using Standards for

various data transfer media (Company, 2011; Intel et al., 2000; Ramamurthy & Ashenayi, 2002; Seifert, 1998).

The first transmission channel represents the medium used to transfer sensor data to a computer which, in the case of the actual flights, was either USB2 or USB3 depending on the sensors' specifications. The second channel tested is from a computer, over a network, to a server, . The third is via either USB2 or USB3, whichever was not used as the initial sensor transmission channel media. Many additional transmission channels, including eSata, FireWire, wireless technologies, and other network/hardware systems exist, and ADAPTTE currently includes the specifications for 30 different channel types and the ability to manually specify a channel/transmission rate. In the context of the transmission capacity validation, however, only the three listed channels were empirically tested.

Transmission timeliness accuracy is a component of the entire model to be validated and is not truly a stand-alone component, therefore, if the modeled data volume is inaccurate, the modeled time required to transfer the inaccurate volume of data will also be inaccurate when compared to the actual transfer times of the actual data. Therefore, the model is run twice, once to estimate the timeliness of data transmission given the actual known data volume, and once to model the timeliness of data transmission given the data volume calculated in the Acquisition Timeliness component. The actual data for each flight was then transferred using the three mentioned transmission channels, on a Dell Precision T1700, and the transmission times recorded.

The difference between the modeled total transmission times across all three channels and the actual transmission times across the three channels forms the basis for assessing

the accuracy of the Transmission Capacity component. This assessment could conceivably account for human-related latencies, as written in the RSCM, but details of those latencies were not available for the actual flights. Additionally, current modes of data transmission, and their inherent bandwidths and latencies are documented in IEEE and USB standards (Company, 2011; Intel et al., 2000; Ramamurthy & Ashenayi, 2002; Seifert, 1998), and these standards are used in ADAPTTE. Actually testing and verifying all extant network technologies and physical media was not possible for this thesis.

3.2.3 Estimating Timeliness for Extant Platform/Sensor Combinations

Information collected from the responding aerial survey firms was used to model information delivery timeliness for all extant platform and sensor combinations for which data from the survey was available. These combinations were then used in conjunction with the locations and dimensions of the six critical infrastructure sites to generate Total Time to Data Delivery estimates for each site, based upon each combination.

$$\boldsymbol{T_{Dat} = T_{Acq} + T_{Chan}} \quad (7)$$

Each platform and sensor combination available, based upon the survey responses, to San Diego County, CA and the State of New Mexico, was modeled for each CI site at 6 centimeters and 12 centimeters Ground Sample Distance. Each sensor was modeled at two levels of compression, high quality TIF or RAW format and JPEG, based upon sensor specifications. Finally, for sensors with exchangeable lenses of varying focal lengths, models were calculated using both a 50mm and a 100mm focal length lens.

3.2.4 Estimating Timeliness for S-UAS Platform/Sensor Combinations

Information collected from the manufacturers' websites about the 3D Robotics Iris+ S-UAS, DJI Spreading Wings 1000+ S-UAS, Canon PowerShot SX260 camera, and Nikon D810 camera was used to model information delivery timeliness for these systems, for the six previously identified critical infrastructure sites. The Iris + was modeled with the PowerShot SX260, and the Spreading Wings was modeled with the Nikon D810 and a 50mm lens. Both systems were modeled for each of the six sites at 6 centimeters and 12 centimeters Ground Sample Distance. With the exception of the North Torrey Pines Bridge site, the S-UAS systems distance to/from the scenes are modeled as though they were located within a building on-site. For the North Torrey Pines Bridge site, since there is not a facility available on-site, the Caltrans District 11 station, 12.6 miles from the bridge is used, and the to/from time modeled as 15 minutes, based upon the Google Maps road network time estimate.

Using methods outlined in Section 3.2.3, T_{Acq} and T_{Chann} are initially calculated for each of the sites. Because S-UAS have the ability to be pre-programmed for use in a swarm, where multiple S-UAS can be deployed to the same region and cover a larger area in a shorter period of time (Daniel et al., 2009), estimates of T_{Dat} for the S-UAS platforms use a sufficient quantity of S-UAS at the site to image the site with each individual S-UAS flying only once. An individual Spreading Wings S-UAS carrying a Nikon D810 and lens has a maximum flight time of 15 minutes, and an individual Iris+ with the Canon Powershot SX260 has a maximum flight time of 12 minutes. The value calculated for T_{Acq} for each platform/sensor combination for each site is then divided by either 15 or 12 minutes, and the number of S-UAS required is the rounded-up result.

Once the number of required S-UAS is known, T_{Acq} is divided by the number of required S-UAS, the resultant value is added to T_{Chann} and the result is T_{Dat}.

4. RESULTS AND DISCUSSION

The results of this work encompass three analyses: the assessment of the accuracy and error bounds of the RSCM, assessment of extant aerial survey firms' capacities to provide time-sensitive remote-sensing services to emergency managers for six critical infrastructure sites, and assessment of the impact of S-UAS on the timeliness of data delivery.

4.1 Model Validation

During the initial process of model validation, the RSCM was found to require revisions.

After the initial model validation results were evaluated. It was observed that both the Sensor Capacity timeliness term and the Bits to Image the Scene term were producing values much lower than the results from the actual field data. A closer inspection of the RSCM revealed the necessity of two changes.

First, Equation 2 applies the compression factor, F, to the calculated number of bits for the given scene area and percent of overlap. This essentially compresses the data volume and the physical scene dimensions. Using the original model, the result led to much faster estimated flight times than what actually occurred with the validation flights. This first revision to the original Equation 2 removes the compression factor from the estimation of Acquisition Capacity (see new Equation 8), and adds it to the original Equation 6, (see new Equation 9).

$$B_S = \left(B_A A_S (1 + E_S)\right) \quad (8)$$

$$T_{Chan} = \sum_i^N 1 \frac{F(B_S)}{C_{Chan,i}} + L_i \quad (9)$$

The second revision to the RSCM, and Equation 2, is to properly account for percent of redundant side lap and overlap. As originally written, E_S is the "percent of redundant acquisition due to side lap and overlap" to which the area of the scene without overlap is added (the value '1'). In order to properly account for redundant acquisition, Equation 2 should be further modified to Equation 10 and Equation 11.

$$B_S = B_A A_S E_S \quad (10)$$

$$E_S = (1 + Sidelap)(1 + Overlap) \quad (11)$$

Following the above revisions to the RSCM, which were necessary in order to conduct a model validation that better fits reality, ADAPTTE and the revised RSCM were ready for the model validation analysis.

4.1.1 Acquisition Capacity

Overall model fit for Acquisition Capacity is highly dependent upon the term T_D, especially for the modeling of manned flights. For 7 out of the 8 manned flights, the value, in seconds, of T_D, was greater than the values of any other individual terms. Figure 6 clearly indicates one of the difficulties encountered in modeling T_D; without access to air route networks, detailed terrain information related to aircraft capabilities, and a

discussion with the pilot prior to modeling travel distances, the chosen alternative was a measurement of Euclidean distance from the airport where the aircraft is located, to the scene. While many aircraft may be technically capable of flying straight paths to a given scene, logistically this was not the case for any of the manned flights used in the validation. A second difficulty encountered in assessing the model accuracy with T_D was the existence of uncertainty concerning the integrity/viability of the validation data from the flights, for T_D. While each of the 8 manned flights had flight path data available in the logs, for each flight the return from scene information either appeared to end in an unpopulated place away from any airport, or it did not exist because the flight management system (e.g., Aviatrix) was powered down prior to the return trip.

The model fit of T_{Acq} for all flights, when including the problematic T_D term, had an Adjusted R^2 value of 0.751 and a Root Mean Squared Error of 49 minutes with an average actual timeliness of acquisition of 126 minutes. See Table 3 for Adjusted R^2 values by term and manned/manned and UAS. By contrast, for just the S-UAS flights, the Adjusted R^2 value was 1.00 and the Root Mean Squared Error was 2 seconds, for flights lasting an average of 8 minutes. Extreme variability in T_D as a result of human control over the flight paths of an aircraft (Figure 13) are not a factor for the S-UAS flights, which flew pre-programmed routes controlled by the Pixhawk autopilot system. These results suggest that coupling ADAPTTE with air traffic routing models would improve the estimation of T_D for manned aircraft.

Excluding T_D from the model assessment results in an Adjusted R^2 value of 0.992 for all flights and an Adjusted R^2 of 0.964 for just the manned flights. The Root Mean

Squared Error for the modeled manned flights was 4.2 minutes for flights lasting an average of 50 minutes when excluding T_D.

Percent Errors for the individual model terms in the estimation of Acquisition Timeliness, B_S/C_{Acq}, T_M, and T_D exhibited varying degrees of fit. Figure 14 summarizes the Percent Errors for the overall timeliness of acquisition, and each of the terms that comprise it. The white boxes in Figure 14 show errors for only manned flights, and the grey boxes show errors for the manned and UAS flights combined. UAS flights are not displayed separately in Figure 14 due to a sample size of 4.

While the median values for B_S/C_{Acq} and T_M fall at or below 20% error, and the median value of T_{Acq} is near 20% error, including the problematic T_D term, there are some notable patterns in the errors. For all terms, the inclusion of the UAS data decreases the median error percent and increases the Adjusted R^2 values. The UAS flights differed substantially from the manned flights in that they were pre-programmed to take off, fly a number of flight lines, and when done, land. Transitions between flight lines, length of flight lines, distances to and from the scene, and aircraft velocity were pre-programmed and not subject to human/pilot interaction. Consequently, it is not surprising that the model's ability to predict the UAS flights' timeliness of acquisitions was substantially better than with manned flights ($R^2 = 0.310$ for manned flights, 1.00 for UAS).

The errors seen in the estimation of T_M ($R^2 = 0.63$ for manned flights, 0.996 for UAS), in particular, suggest that the autonomy of a human pilot is a source of error in the model. The inclusion of four UAS flights to the eight manned flights causes the median error percent of T_M to decrease from 11.2% to 5.5%. T_M is the transition time between flight lines, which is a factor of the aircraft velocity while transitioning, and the distances

of the transitions. While the python implementation of the RSCM attempts to predict the required turn radius and heading changes for different aircraft, it does so using purely mathematical assumptions of an aircraft's abilities. For manned flights, the transition curves and distances are determined by the pilot of the aircraft, not software, and are not programmed into an auto-pilot. Figure 8 shows examples of flight line transition variability related to human control of the aircraft. The implementation of RSCM used in this study attempts to model the average, normal transition curves shown in Figure 15 as Transition 1, but is unable to account for transition curves like those shown in Transition 7. The average time required to fly each of the transitions shown in Figure 15 was 88 seconds, with Transition 7, the maximum value and an outlier, taking 154 seconds, and Transition 10 (not shown) having the second highest value, at 114 seconds. With the transitions 7 and 10 excluded from the mean value of T_M, the average time of the actual flight line transitions changes from 88 seconds to 82 seconds. The model estimate had an average transition time of 79 seconds (3 seconds difference). This pattern of transition times varying due to one, two, or more non-standard transition paths in a flight exists within each of the eight manned flights used in this study.

4.1.2 Transmission Capacity

Overall model fit for Transmission Capacity, using the actual data volume values within the model had an Adjusted R^2 value of 0.987 and an RMSE of 199 seconds. The model fit when using the modeled data volume values with the actual data volume transmission times produced an Adjusted R^2 of 0.997 and an RMSE of 77 seconds. See Tables 4 for the Transmission Capacity information.

It is important to note that the high accuracy values of the transmission capacity analysis do not take into consideration the human factors that certainly would contribute to the latency term for each channel, *L*. As previously noted in the Acquisition Capacity results, human factors can be a substantial source of variability and therefore model error.

4.2 Aerial Survey Firm Results by Platform/Sensor Combination and Site

The three example critical infrastructure locations in Southern California are the San Vicente Dam, the Del Mar Pump Station, and the North Torrey Pines Bridge. For each of these three sites the platform/sensor combination of the Cessna T206 using the Nikon D800 Camera with a 50mm lens yielded the shortest T_{Dat} estimates. Given a Ground Sample Distance of 6cm, this combination could deliver imagery from the San Vicente Dam in 3.16 hours, from the Del Mar Pump Station in 2.8 hours, and from the North Torrey Pines Bridge in 2.84 hours. See Table 5 for additional estimates by platform/sensor for these sites at 6cm GSD. At 12cm Ground Sample Distance, this combination could deliver imagery from the San Vicente Dam in 3.05 hours, from the Del Mar Pump Station in 2.8 hours, and from the North Torrey Pines Bridge in 2.82 hours. See Table 6 for additional estimate by platform/sensor for these sites at 12cm GSD.

The three example critical infrastructure locations in New Mexico are the South Capital Complex, Cochiti Lake, and the Sandoval Detention Center. The Cessna 182 with the Canon 6D yields the shortest T_{Dat} for each of the three sites. Given a Ground Sample Distance of 6cm, this combination could deliver imagery from the South Capital Complex in 1.41 hours, from the Cochiti Lake in 4 hours, and from the Sandoval Detention Center in 0.78 hours. See Table 7 for additional estimates by platform/sensor

for these sites at 6cm GSD. At 12cm Ground Sample Distance, this combination could deliver imagery from the South Capital Complex in 1.3 hours, from the Cochiti Lake in 2.29 hours, and from the Sandoval Detention Center in 0.74 hours. See Table 8 for additional estimate by platform/sensor for these sites at 12cm GSD.

Due to the fact that only one survey respondent's aircraft and sensor are located in New Mexico, the combination of the Cessna 182 with a Canon 6D camera outperforms the other two available platform/sensor combinations by over six hours for the South Capital Complex and Sandoval County Detention Center sites. Due in part to the slower available sensor transmission channels of the Canon 6D compared to the UltraCam X and Intergraph DMC1, the larger overall area of the Cochiti Lake compared with the other two sites, and the smaller sensor size of the Canon 6D compared with the UltraCam X and Intergraph DMC1, the timeliness estimates for the for those two sensors and associated aircraft are within 3 hours of the estimates for the Canon 6D. Both the Piper Navajo with the DMC1 and the Cessna TU206G with the UltraCam X are capable of acquiring imagery in four-bands, whereas the Canon 6D acquires only three bands. Although not explicitly stated in the online survey answers, it is conceivable that the operators of the two platforms/sensors not physically located in New Mexico could acquire imagery at CI sites in New Mexico, land at a local nearby airport, and transfer the data prior to returning to their airports of origin. Because the estimates used in the model for time to travel to and from the scene makes the assumption that the aircraft would return to its home facility, an operator willing to land closer to the sites of interest could effectively reduce the total timeliness estimate for data delivery.

4.3 S-UAS Results by Site

For each of the three sites in Southern California, the two S-UAS platform/sensor combination swarms had T_{Dat} estimates within 3 minutes of each another. As noted in Section 3.2.4, the value of T_{Dat} for these swarms will be near the maximum flight time of an individual S-UAS from a given platform/sensor combination. With this in mind, the greatest variation for the S-UAS systems is in the number of S-UAS required for a site. Given a Ground Sample Distance of 6cm, a swarm of 3 Spreading Wings 1000's (S1000s) with Nikon D810 cameras and 50mm lenses could deliver imagery from the San Vicente Dam in 0.23 hours, 2 S1000's or 2 Iris+'s with Canon Powershot SX260 cameras could deliver imagery from the Del Mar Pump Station in 0.18 hours, and 2 S1000's could deliver imagery from the North Torrey Pines Bridge in 0.44 hours. See Table 9 for additional timeliness and S-UAS swarm size estimates for these sites at 6cm GSD. Given a Ground Sample Distance of 12cm, 3 S1000's could deliver imagery from the San Vicente Dam in 0.2 hours, 2 S1000's or 2 Iris+'s could deliver imagery from the Del Mar Pump Station in 0.2 hours and 0.19 hours, and 2 S1000's or 2 Iris+'s could deliver imagery from the North Torrey Pines Bridge in 0.45 hours. See Table 10 for additional timeliness and S-UAS swarm size estimates for these sites at 12cm GSD.

For each of the three sites in New Mexico, the two S-UAS platform/sensor combination swarms also had T_{Dat} estimates within 3 minutes of each another. Given a Ground Sample Distance of 6cm, a swarm of 3 S1000s with Nikon D810 cameras and 50mm lenses could delivery imagery from the South Capital Complex in 0.19 hours, 21 SW1000's could deliver imagery from the Cochiti Lake in 0.46 hours, and 2 S1000's could deliver imagery from the Sandoval Detention Center in 0.2 hours. See Table 11 for

additional timeliness and S-UAS swarm size estimates for these sites at 6cm GSD. Given a Ground Sample Distance of 12cm, 3 S1000's could deliver imagery from the South Capital Complex in 0.17 hours, 12 S1000's could deliver imagery from the Cochiti Lake in 0.3 hours, and 2 S1000's could deliver imagery from the Sandoval Detention Center in 0.21 hours. See Table 12 for additional timeliness and S-UAS swarm size estimates for these sites at 12cm GSD.

4.4 Limitations of These Results

Specific limitations of the results of this research were discussed along with the results. Model validation results were derived from 8 manned and 4 unmanned flights, and while the Adjusted R^2 and RMSE values show a strong fit between what the RSCM predicts and the actual flight values for terms T_{Acq}, B_S/C_{Acq}, T_M and T_{Chann}, access to and incorporation of additional manned/unmanned flights and platform/sensor combinations could be useful in further refining the error bounds of the RSCM. Having access to flight data where the integrity of the T_D term is not compromised by the logging hardware being shutdown immediately after image acquisition could improve the model fit for that term. Human-related latencies are not evaluated in the model validation of Transmission Capacity, which would result in an increase in the error of Transmission Capacity.

The extant platform timeliness assessments for each of the six critical infrastructure sites were based upon the results from the aerial survey firms that chose to participate in our survey, which totaled 31% of the online survey requests sent to eligible firms. Particularly, those firms which actively declined to participate in the survey could potentially provide more timely platform/sensor combinations for the evaluated critical infrastructure sites.

5. CONCLUSIONS

The ability to assess the timeliness of TSRSS is critical to the configuration and incorporation of these systems into emergency managers' and management organizations' standard operating procedures (C. Lippitt et al., 2015). The RSCM was created, in part, to provide a means for assessing the timeliness of information delivery under various RSS configurations. Automation of RSCM capacity analysis through ADAPTTE makes the estimation of acquisition and transmission timeliness in the RSS design phase routine, but also enables on-the-fly estimation of data delivery time (T_{Dat}) to aid in asset tasking (i.e., dynamic RSS configuration) during the response phase of the hazard cycle. This thesis answers three questions related to the use of the RSCM for providing timeliness assessments of extant systems and configuring hypothetical systems.

The first question, "How accurately can the timeliness of airborne data acquisition and delivery be estimated, using the Remote Sensing Communication Model Capacity Analysis?" is answered by the results in Section 4.1.1. Eight manned and four unmanned flights were used to empirically test the predictions from the RSCM. For manned platform systems, given the complications of calculating the time to move the platform to and from the scene, an RMSE of 60 minutes is observed for Acquisition Capacity, and an RMSE of 1.3 minutes is observed for Transmission Capacity. The results clearly indicate improved model fit when human pilots are not directly operating the aircraft platform but also suggest that integration of addition information affecting T_{D} (e.g., airspace information, ground elevation data).

The second question, "Using RSCM Capacity Analysis, what is the estimated data delivery timeliness of extant aerial survey firms in support of a remote sensing system for

hazard response in New Mexico and San Diego County, CA?" is answered by the results in Section 4.2. The online survey results from six aerial survey companies were used to estimate extant platform/sensor combinations in support of hazard response at six potentially critical infrastructure sites. In San Diego County the following sites were used: San Vicente Dam, Del Mar Pump Station, North Torrey Pines Bridge. In New Mexico the following sites were used: South Capital Complex, Cochiti Lake, Sandoval Detention Center. The results in Table 5, Table 6, Table 7, and Table 8 show timeliness estimates by platform/sensor configuration and Ground Sample Distance for the extant aerial survey firms.

The third question, "How will the introduction of UAS affect data delivery timeliness?" is answered by the results in Section 4.3. Two S-UAS platform/sensor combinations were evaluated, using multiple S-UAS in a swarm at each site, for each of the six critical infrastructure sties. Assuming on-site location of the systems, for the two platforms evaluated, this amounted to 15 minutes, and 12 minutes, per site. Transmission Capacity of these systems was dependent upon whether images were to be captured in Raw or JPEG format, and whether the sensor uses USB 2 or USB 3 for its primary transmission channel. The range of transmission times was from less than 1 minute to 27 minutes, dependent upon the size of the area and sensor/format used. These results show that the introduction of S-UAS could have the potential for reducing data delivery times by: having the systems located at or near the sites, having a sufficient number of systems in a swarm to cover an area in one flight per platform, and configuring the systems to meet the spatial/spectral needs of the emergency manager/organization. This is best demonstrated by a comparison of the shortest Time to Data Delivery (T_{Dat}) estimates.

Using the San Vicente Dam as the example, the shortest manned platform T_{Dat} was 3.05 hours at 12cm GSD, whereas with 3 Spreading Wings 1000 S-UAS platforms operating simultaneously, the San Vicente Dam could be imaged at 6cm GSD in 14 minutes.

This research clearly demonstrates that the RSCM can be used for modeling the acquisition and transmission timeliness of dynamically configurable RSS. Additionally, the capacity for aerial survey firms to provide timely information about sites in San Diego County, CA and Central/Northern New Mexico ranges from ~1 to ~4 hours for the three band sensors, and ~2 to ~6 hours for the four band sensors. Using a sufficient number of S-UAS in a swarm configuration to cover an entire area has the possibility of substantially reducing these estimates, to slightly over the maximum flight time for a single given S-UAS.

6. BIBLIOGRAPHY

Bruzewicz, A. J. (2003). *Remote Sensing Imagery for Emergency Management. In: The Geographical Dimensions of Terrorism*.

Colomina, I., & Molina, P. (2014). Unmanned aerial systems for photogrammetry and remote sensing: A review. *ISPRS Journal of Photogrammetry and Remote Sensing*, *92*, 79–97. doi:10.1016/j.isprsjprs.2014.02.013

Company, H. (2011). *Universal Serial Bus 3 . 0 Specification*. *ReVision*. Retrieved from http://www.usb.org/developers/docs/usb_31_010516.zip

Cutter, S. L. (2003). GI Science , Disasters , and Emergency Management. *Transactions in GIS*, *7*(4), 439–445.

Daniel, K., Dusza, B., Lewandowski, A., Wietfeld, C., & De, C. W. (2009). AirShield : A System-of-Systems MUAV Remote Sensing Architecture for Disaster Response. In *IEEE International Systems Conference*.

Dashora, A., & Lohani, B. (2013). Turning mechanisms for airborne LiDAR and photographic data acquisition. *Journal of Applied Remote Sensing*, *7*(1). doi:10.1117/1.JRS.7.073488

Eguchi, R., & Huyck, C. (2001). Resilient disaster response: using remote sensing technologies for post-earthquake damage detection. *Earthquake Engineering to Extreme Events (MCEER), Research Progress and Accomplishments*, 125–137. Retrieved from http://mceer.buffalo.edu/publications/resaccom/03-SP01/09eguchi.pdf

Ehrlich, D., Guo, H. D., Molch, K., Ma, J. W., & Pesaresi, M. (2009). Identifying damage caused by the 2008 Wenchuan earthquake from VHR remote sensing data.

International Journal of Digital Earth, *2*(4), 309–326. doi:10.1080/17538940902767401

George, S. (2015). FAA unmanned aircraft systems (UAS): Overview: UAS and the proposed small UAS rule. *Integrated Communication, Navigation, and Surveillance Conference*, 1–28. doi:10.1109/ICNSURV.2015.7121361

Gitas, I. Z., Polychronaki, A., Katagis, T., & Mallinis, G. (2008). Contribution of remote sensing to disaster management activities: A case study of the large fires in the Peloponnese, Greece. *International Journal of Remote Sensing*, *29*(6), 1847–1853. doi:10.1080/01431160701874553

Intel, Compaq, Hewlett-packard, Microsoft, Lucent, Philips, & C, N. E. (2000). *Universal Serial Bus Specification*. *Group*. Retrieved from http://www.usb.org/developers/docs/usb_20_071411.zip

Jeyaseelan, A. (2003). Droughts & Floods Assessment and Monitoring Using Remote Sensing and GIS. *Satellite Remote Sensing and GIS Applications in Agricultural Meteorology*, 291–313. Retrieved from http://www.wamis.org/agm/pubs/agm8/Paper-14.pdf

Joyce, K. E., Belliss, S. E., Samsonov, S. V., McNeill, S. J., & Glassey, P. J. (2009). A review of the status of satellite remote sensing and image processing techniques for mapping natural hazards and disasters. *Progress in Physical Geography*, *33*(2), 183–207. doi:10.1177/0309133309339563

Laben, C. (2002). Integration of remote sensing data and geographic information system technology for emergency managers and their applications at the Pacific Disaster Center. *Optical Engineering*, *41*(9), 2129. doi:10.1117/1.1501137

Laituri, M., & Kodrich, K. (2008). On Line Disaster Response Community: People as Sensors of High Magnitude Disasters Using Internet GIS. *Sensors*, *8*(5), 3037–3055. doi:10.3390/s8053037

Lippitt, C. D. (2015). PERSPECTIVES FROM THE FIELD: Remote Sensing from Small Unmanned Platforms: A Paradigm Shift. *Environmental Practice*, *17*(03), 235–236. doi:10.1017/S1466046615000204

Lippitt, C. D., & Stow, D. A. (2015). Remote Sensing Theory and Time-Sensitive Information. In *Time-Sensitive Remote Sensing* (pp. 1–10). Springer.

Lippitt, C. D., Stow, D. A., & Clarke, K. C. (2014). On the Nature of Models For Time- - - Sensitive Remote Sensing * Corresponding author . Email : clippitt@unm.edu Abstract. *International Journal of Remote Sensing*, *35*(18), 6815–6841.

Lippitt, C., Stow, D., & Coulter, L. (2015). *Time-Sensitive Remote Sensing*. New York: Springer.

Maddalon, J. M., Hayhurst, K. J., Morris, A., & Verstynen, H. (2013). Considerations of Unmanned Aircraft Classification for Civil Airworthiness Standards. *AIAA Infotech@Aerospace (I@A) Conference*, (February), 1–16. doi:10.2514/6.2013-5216

Metternicht, G., Hurni, L., & Gogu, R. (2005). Remote sensing of landslides: An analysis of the potential contribution to geo-spatial systems for hazard assessment in mountainous environments. *Remote Sensing of Environment*, *98*(2-3), 284–303. doi:10.1016/j.rse.2005.08.004

Niethammer, U., James, M. R., Rothmund, S., Travelletti, J., & Joswig, M. (2012). UAV-based remote sensing of the Super-Sauze landslide: Evaluation and results. *Engineering Geology*, *128*, 2–11. doi:10.1016/j.enggeo.2011.03.012

Phinn, S. R. (1998). A framework for selecting appropriate remotely sensed data dimensions for environmental monitoring and management. *International Journal of Remote Sensing*, *19*(17), 3457–3463.

Phinn, S. R., Stow, D. A., Franklin, J., Mertes, L. A. K., & Michaelsen, J. (2003). Remotely Sensed Data for Ecosystem Analyses: Combining Hierarchy Theory and Scene Models. *Environmental Management*, *31*(3), 429–441. doi:10.1007/s00267-002-2837-x

Ramamurthy, G., & Ashenayi, K. (2002). Comparative study of the FireWire™ IEEE-1394 protocol with the Universal Serial Bus and Ethernet. In *Circuits and Systems, 2002. MWSCAS-2002. The 2002 45th Midwest Symposium on* (Vol. 2, pp. II–509).

Seifert, R. (1998). *Gigabit Ethernet: technology and applications for high-speed LANs*. Addison-Wesley Longman Publishing Co., Inc.

Smith, M., Chandler, J., & Rose, J. (2009). High spatial resolution data acquisition for the geosciences: kite aerial photography. *Earth Surface Processes and Landforms*, *34*, 155–161. doi:10.1002/esp

Strahler, A. H., Woodcock, C. E., & Smith, J. A. (1986). On the nature of models in remote sensing. *Remote Sensing of Environment*, *20*(2), 121–139. doi:10.1016/0034-4257(86)90018-0

Turner, W., Spector, S., Gardiner, N., Fladeland, M., Sterling, E., & Steininger, M. (2003). Remote sensing for biodiversity science and conservation. *Trends in Ecology & Evolution*, *18*(6), 306–314. doi:10.1016/S0169-5347(03)00070-3

Watts, A. C., Ambrosia, V. G., & Hinkley, E. a. (2012). Unmanned aircraft systems in remote sensing and scientific research: Classification and considerations of use.

Remote Sensing, *4*, 1671–1692. doi:10.3390/rs4061671

Westoby, M. J., Brasington, J., Glasser, N. F., Hambrey, M. J., & Reynolds, J. M. (2012). "Structure-from-Motion" photogrammetry: A low-cost, effective tool for geoscience applications. *Geomorphology*, *179*, 300–314. doi:10.1016/j.geomorph.2012.08.021

Zhang, S., Lippitt, C. D., Bogus, S. M., Loerch, A. C., & Sturm, J. O. (2016). The accuracy of aerial triangulation products automatically generated from hyper-spatial resolution digital aerial photography. *Remote Sensing Letters*, *7*(2), 160–169. doi:10.1080/2150704X.2015.1121299

Zhang, S., Lippitt, C. D., Chen, C., Bogus, S. M., Lippitt, C. D., Neville, P. R. H., … Valentin, V. (2015). Extracting pavement distress condition patterns based on high spatial resolution multispectral digital aerial photography . Extracting Pavement Surface Distress Conditions Based on High Spatial Resolution Multispectral Digital Aerial Photography. *Photogrammetric Engineering & Remote Sensing*, *81*(9), 700–720. doi:10.14358/PERS.81.9.709

7. TABLES

Table 1: RSCM Variable definitions and sources.

Variable	Description	Source
Reg	Targeted region	Selected from lists of Critical Infrastructure sites
D_{Reg}	Distance from aircraft location to targeted region	Derived from survey question "where is your aircraft located", and for S-UAS, at the site.
T_D	Time to fly platform to targeted region	Derived from platform make/model velocity and D_{Reg}
T_M	Time to transition between flight lines	Derived from flight line spacing, number of flight lines, and aircraft velocity
N	Number of flight lines to cover region	Derived from Aviatrix/Mission Planner flight-planning software and based on the area of Reg
F	Compression factor used by imaging sensor	Derived from sensor make/model.
A_S	The total area of the targeted region	Derived from Reg
E_S	Percentage of redundant overlap	Derived from the flight-line planning using Aviatrix/Mission Planner software.
R_G	Desired Ground Sampling Distance	This will be based on somewhere between 1-6 inches GSD for each region.
B_P	# of bits required to store a pixel	Derived from the bit-depth and file format of the images created by the imaging sensors
D_W	Swath width in Ground Distance	Derived from the altitude of the aircraft/S-UAS and the size of the imaging sensor. This information was generated through a combination of Aviatrix/Mission Planner flight planning and survey answers
V	Aircraft velocity during acquisition	Derived from aircraft/S-UAS make/model, imaging sensor capabilities, and flight logs
C_{Chan}	Channel transmission capacity in bits per unit time	Derived from the data transfer/transmission capabilities of the methods/services listed in the survey answers, which apply to S-UAS as well
L	Latencies in data transmission	Human and technical latencies derived from information in the survey answers and inherent in the transmission technologies used.

Table 2: Extant Platform/Sensor Combinations

Platform	Location	Sensor
Cessna T206	Southern California	
		Nikon D800
		Canon 5D Mark III
Cessna TU206G	Central Arizona	
		Vexcell Ultracam X
Cessna 320D	Southern California	
		MS Ultracam Falcon Prime
Piper Navajo Chieftain	Southern California	
		Intergraph DMC 1
Beechcraft Bonanza	Southern California	
		Intergraph DMC 2
Cessna 182	Central New Mexico	
		Canon 6D
Piper Navajo	Northeast Kansas	
		Intergraph DMC 1

Table 3: RSCM Acquisition Capacity Model Fit

Variable	Manned Only R^2_{adj}	Manned Only MPE	Manned & UAS R^2_{adj}	Manned & UAS MPE
T_{Acq}	0.310	31	0.751	21
B_S/C_{Acq}	0.953	11	0.985	7
T_M	0.686	16	0.937	11
T_D	0.053	53	0.409	36

Table 4: RSCM Transmission Capacity Model Fit

Variable	(R^2_{adj})	MPE (%)
T_{Chann}: Modeled Volume	0.997	9
T_{Chann}: Actual Volume	0.987	13

Table 5: Timeliness Estimates for Sites in San Diego County, CA at 6cm GSD

				San Vicente Dam			Del Mar Pump Station			North Torrey Pines Bridge		
Platform	**Sensor**	**Bit Depth**	**Bands**	**Tdat (h)**	**Tacq (m)**	**Tchan (m)**	**Tdat (h)**	**Tacq (m)**	**Tchan (m)**	**Tdat (h)**	**Tacq (m)**	**Tchan (m)**
Cessna T206	D800 - 100mm	14	3	3.17	129	61	2.80	108	60	2.84	110	60
	D800 - 100mm	8	3	3.16	129	61	2.80	108	60	2.83	110	60
	5D Mark III - 100mm	14	3	3.29	133	65	2.80	108	60	2.84	110	60
	5D Mark III - 100mm	8	3	3.26	133	63	2.80	108	60	2.84	110	60
Cessna 320D	Ultracam FP - 100mm	12	4	4.15	129	120	3.96	117	120	3.97	118	120
	Ultracam FP - 100mm	8	3	4.15	129	120	3.96	117	120	3.97	118	120
Piper Navajo Chieftain	DMC 1 - 120mm	12	4	3.41	85	120	3.22	73	120	3.24	74	120
	DMC 1 - 120mm	8	3	3.41	85	120	3.22	73	120	3.24	74	120
Beechcraft Bonanza	DMC 2 - 92mm	14	4	3.42	85	120	3.23	74	120	3.25	75	120
	DMC 2 - 92mm	8	3	3.41	85	120	3.23	74	120	3.25	75	120
Cessna TU206G	Ultracam X - 100mm	12	4	6.71	282	120	6.83	290	120	6.83	290	120
	Ultracam X - 100mm	8	3	6.74	282	120	6.83	290	120	6.83	290	120

Table 6: Timeliness Estimates for Sites in San Diego County, CA at 12cm GSD

				San Vicente Dam			Del Mar Pump Station			North Torrey Pines Bridge		
Platform	**Sensor**	**Bit Depth**	**Bands**	**Tdat (h)**	**Tacq (m)**	**Tchan (m)**	**Tdat (h)**	**Tacq (m)**	**Tchan (m)**	**Tdat (h)**	**Tacq (m)**	**Tchan (m)**
Cessna T206	D800 - 100mm	14	3	3.06	123	60	2.80	108	60	2.82	109	60
	D800 - 100mm	8	3	3.05	123	60	2.80	108	60	2.82	109	60
	5D Mark III - 100mm	14	3	3.11	125	61	2.80	108	60	2.82	109	60
	5D Mark III - 100mm	8	3	3.10	125	61	2.80	108	60	2.82	109	60
Cessna 320D	Ultracam FP - 100mm	12	4	4.11	126	120	3.95	117	120	3.97	118	120
	Ultracam FP - 100mm	8	3	4.11	126	120	3.95	117	120	3.97	118	120
Piper Navajo Chieftain	DMC 1 - 120mm	12	4	3.36	81	120	3.21	73	120	3.23	74	120
	DMC 1 - 120mm	8	3	3.35	81	120	3.21	73	120	3.23	74	120
Beechcraft Bonanza	DMC 2 - 92mm	14	4	3.36	82	120	3.23	74	120	3.25	75	120
	DMC 2 - 92mm	8	3	3.36	82	120	3.23	74	120	3.25	75	120
Cessna TU206G	Ultracam X - 100mm	12	4	6.65	279	120	6.83	290	120	6.83	290	120
	Ultracam X - 100mm	8	3	6.65	279	120	6.83	290	120	6.83	290	120

Table 7: Timeliness Estimates for Sites in New Mexico at 6cm GSD

				South Capital Complex			Cochiti Lake			Sandoval Detention Center		
Platform	**Sensor**	**Bit Depth**	**Bands**	**Tdat (h)**	**Tacq (m)**	**Tchan (m)**	**Tdat (h)**	**Tacq (m)**	**Tchan (m)**	**Tdat (h)**	**Tacq (m)**	**Tchan (m)**
Cessna TU206G	Ultracam X - 100mm	12	4	8.04	362	120	8.63	394	123	7.53	332	120
	Ultracam X - 100mm	8	3	8.04	362	120	8.60	394	122	7.53	332	120
Cessna 182	Canon 6D - 100mm	14	3	1.43	83	2	4.55	198	76	0.78	46	0
	Canon 6D - 100mm	8	3	1.41	83	1	4.00	198	42	0.78	46	0
Piper Navajo	DMC 1 - 120mm	12	4	8.70	402	120	9.72	459	123	8.99	419	120
	DMC 1 - 120mm	8	3	8.70	402	120	9.69	459	122	8.99	419	120

Table 8: Timeliness Estimates for Sites in New Mexico at 12cm GSD

				South Capital Complex			Cochiti Lake			Sandoval Detention Center		
Platform	**Sensor**	**Bit Depth**	**Bands**	**Tdat (h)**	**Tacq (m)**	**Tchan (m)**	**Tdat (h)**	**Tacq (m)**	**Tchan (m)**	**Tdat (h)**	**Tacq (m)**	**Tchan (m)**
Cessna TU206G	Ultracam X - 100mm	12	4	8.00	360	120	8.12	367	120	7.51	331	120
	Ultracam X - 100mm	8	3	8.00	360	120	8.13	367	121	7.51	331	120
Cessna 182	Canon 6D - 100mm	14	3	1.31	78	1	2.43	127	19	0.74	44	0
	Canon 6D - 100mm	8	3	1.30	78	0	2.29	127	11	0.74	44	0
Piper Navajo	DMC 1 - 120mm	12	4	8.66	400	120	9.19	431	120	8.97	418	120
	DMC 1 - 120mm	8	3	8.66	400	120	9.20	431	121	8.97	418	120

Table 9: S-UAS Timeliness Estimates for Sites in San Diego County, CA at 6cm GSD

			San Vicente Dam				Del Mar Pump Station				North Torrey Pines Bridge			
Platform	**Sensor**	**Bit Depth**	**# of UAS**	**Tdat (h)**	**Tacq (m)**	**Tchan (m)**	**# of UAS**	**Tdat (h)**	**Tacq (m)**	**Tchan (m)**	**# of UAS**	**Tdat (h)**	**Tacq (m)**	**Tchan (m)**
S1000	D810 - 50mm	14	3	0.23	42	1	2	0.18	22	0	2	0.44	53	0
	D810 - 50mm	8	3	0.23	42	1	2	0.18	22	0	2	0.44	53	0
Iris+	SX260	8	8	0.19	93	2	2	0.18	22	0	3	0.38	68	0

Table 10: S-UAS Timeliness Estimates for Sites in San Diego County, CA at 12cm GSD

			San Vicente Dam				Del Mar Pump Station				North Torrey Pines Bridge			
Platform	**Sensor**	**Bit Depth**	**# of UAS**	**Tdat (h)**	**Tacq (m)**	**Tchan (m)**	**# of UAS**	**Tdat (h)**	**Tacq (m)**	**Tchan (m)**	**# of UAS**	**Tdat (h)**	**Tacq (m)**	**Tchan (m)**
S1000	D810 - 50mm	14	3	0.2	35	0	2	0.2	24	0	2	0.45	54	0
	D810 - 50mm	8	3	0.19	35	0	2	0.2	24	0	2	0.45	54	0
Iris+	SX260	8	5	0.22	62	0	2	0.19	22	0	2	0.45	54	0

Table 11: S-UAS Timeliness Estimates for Sites in New Mexico at 6cm GSD

			South Capital Complex				Cochiti Lake				Sandoval Detention Center			
Platform	**Sensor**	**Bit Depth**	**# of UAS**	**Tdat (h)**	**Tacq (m)**	**Tchan (m)**	**# of UAS**	**Tdat (h)**	**Tacq (m)**	**Tchan (m)**	**# of UAS**	**Tdat (h)**	**Tacq (m)**	**Tchan (m)**
S1000	D810 - 50mm	14	3	0.19	33	1	21	0.62	310	23	2	0.20	24	0
	D810 - 50mm	8	3	0.19	33	0	21	0.46	310	13	2	0.20	24	0
Iris+	SX260	8	5	0.21	60	1	95	0.65	1135	27	3	0.16	29	0

Table 12: S-UAS Timeliness Estimates for Sites in New Mexico at 6cm GSD

			South Capital Complex				Cochiti Lake				Sandoval Detention Center			
Platform	**Sensor**	**Bit Depth**	**# of UAS**	**Tdat (h)**	**Tacq (m)**	**Tchan (m)**	**# of UAS**	**Tdat (h)**	**Tacq (m)**	**Tchan (m)**	**# of UAS**	**Tdat (h)**	**Tacq (m)**	**Tchan (m)**
S1000	D810 - 50mm	14	3	0.17	30	0	12	0.34	176	6	2	0.21	25	0
	D810 - 50mm	8	3	0.17	30	0	12	0.30	176	3	2	0.21	25	0
Iris+	SX260	8	4	0.19	44	0	50	0.31	596	7	3	0.15	27	0

8. FIGURES

Figure 1: Graphic depiction of the RSCM

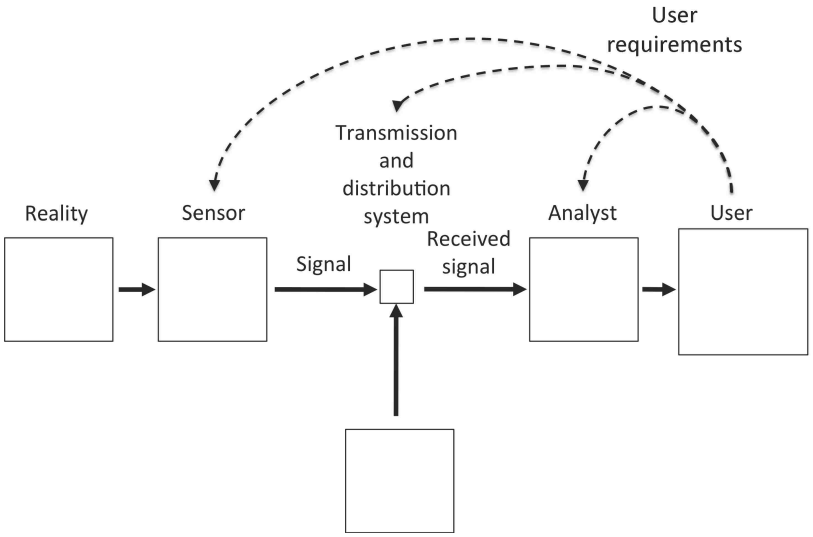

Figure 2: Validation Site

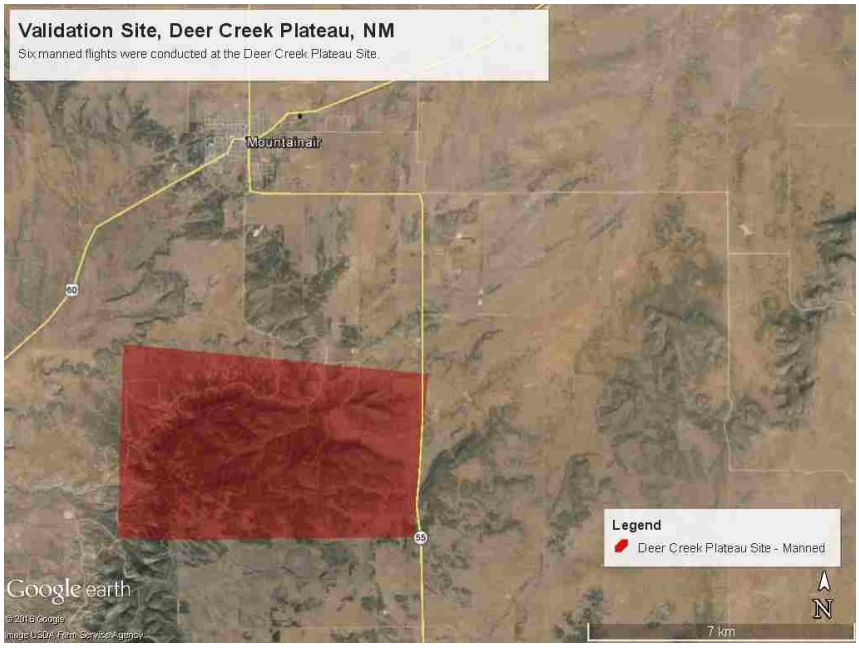

Figure 3: Validation Site

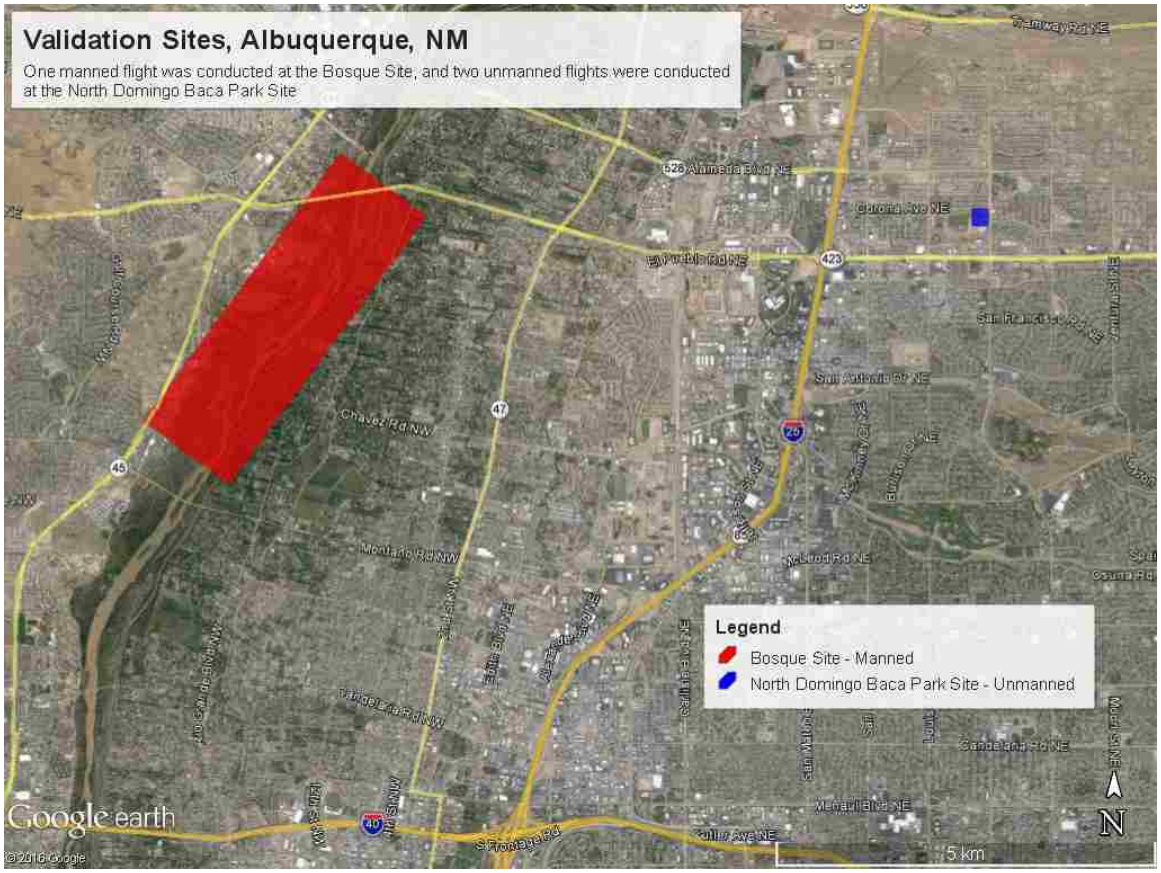

Figure 4: Validation Site

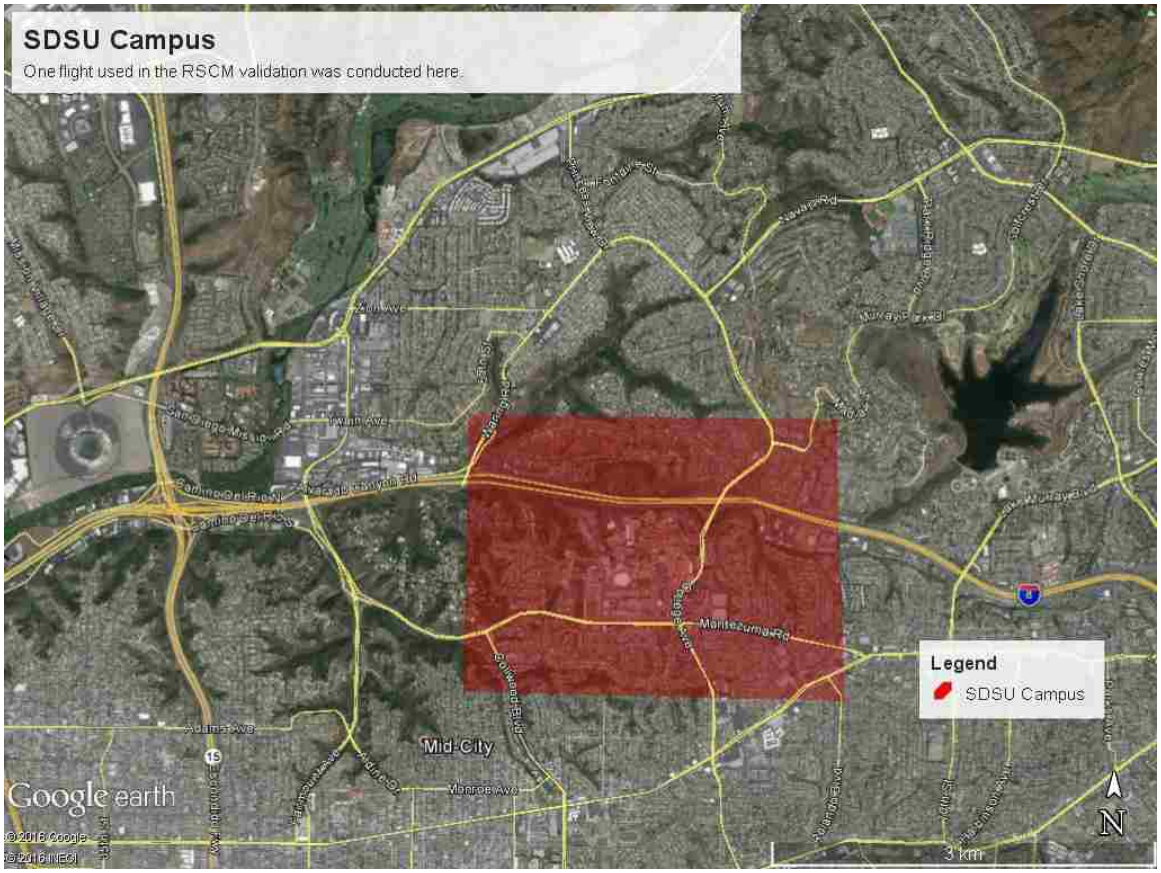

Figure 5: Validation Site

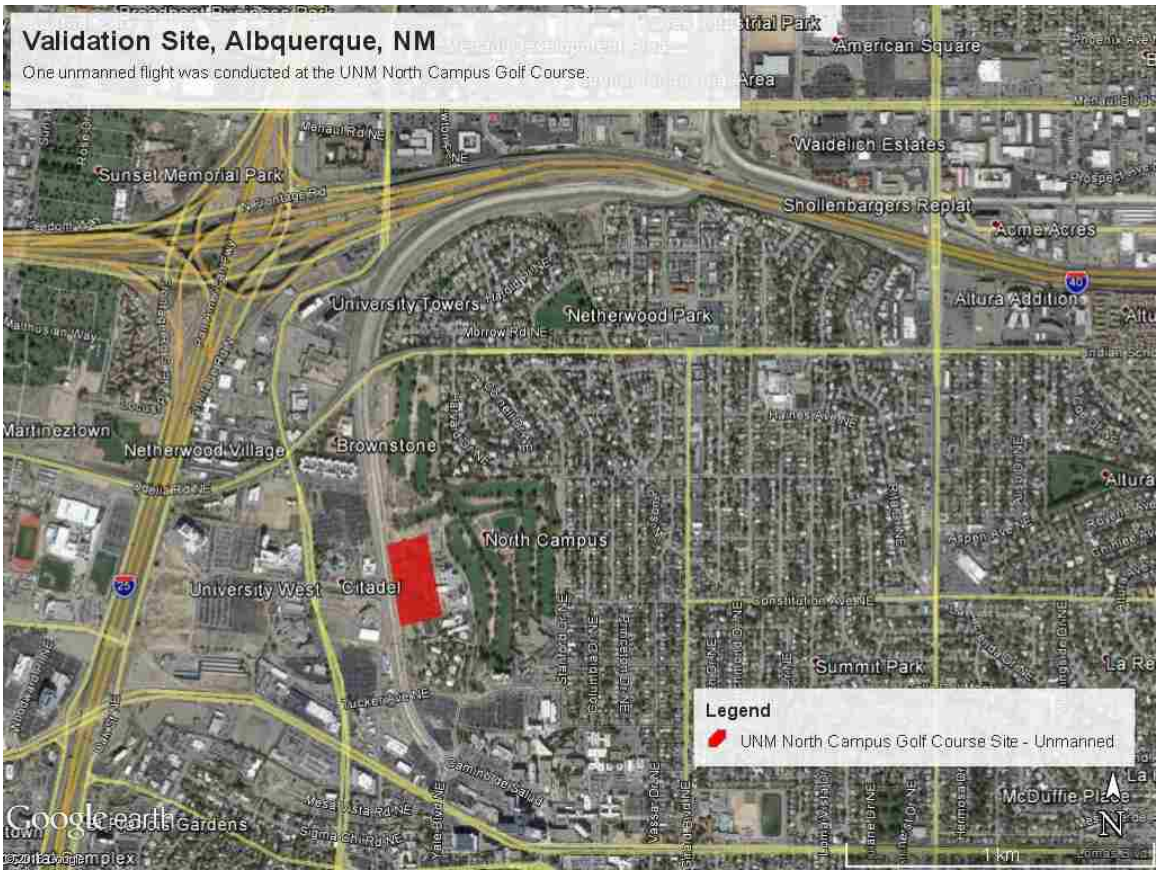

Figure 6: Validation Site

Figure 7: Example Critical Infrastructure Site, San Diego County, CA

Figure 8: Example Critical Infrastructure Site, San Diego County, CA

Figure 9: Example Critical Infrastructure Site, San Diego County, CA

Figure 10: Example Critical Infrastructure Site, Santa Fe County, NM

Figure 11: Example Critical Infrastructure Site, Sandoval County, NM

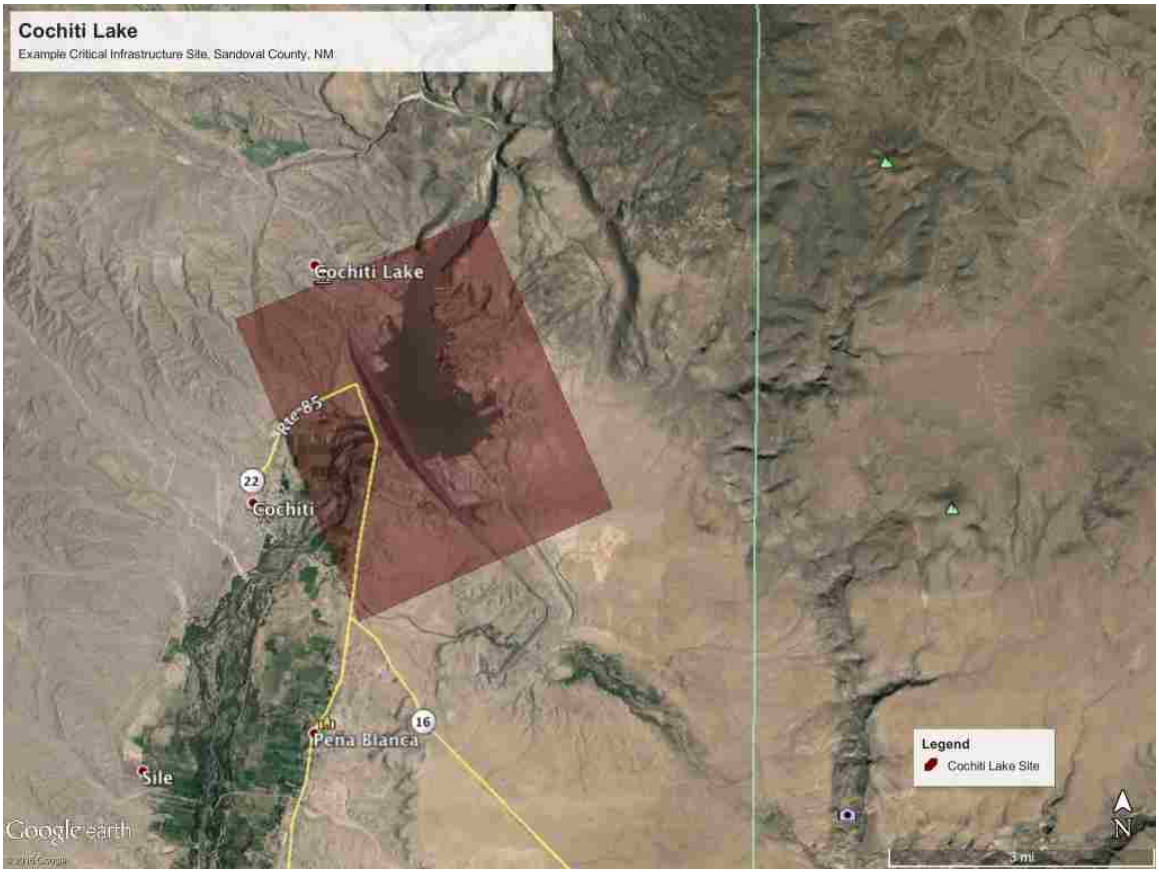

Figure 12: Example Critical Infrastructure Site, Sandoval County, NM

Figure 13: Example of T_D Deviation from Euclidean Distance Model

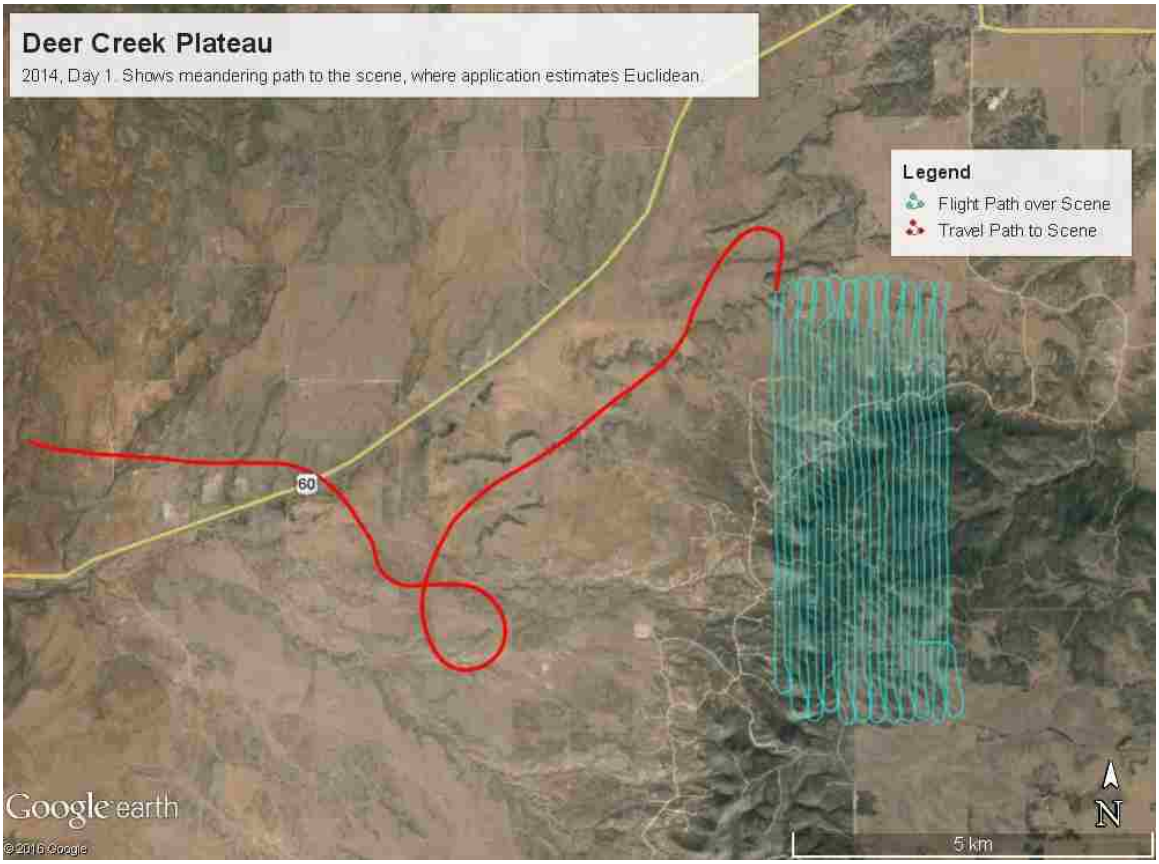

Figure 14: Percent Error by Acquisition Capacity Term. White boxes are Manned Only, Gray are Manned & UAS

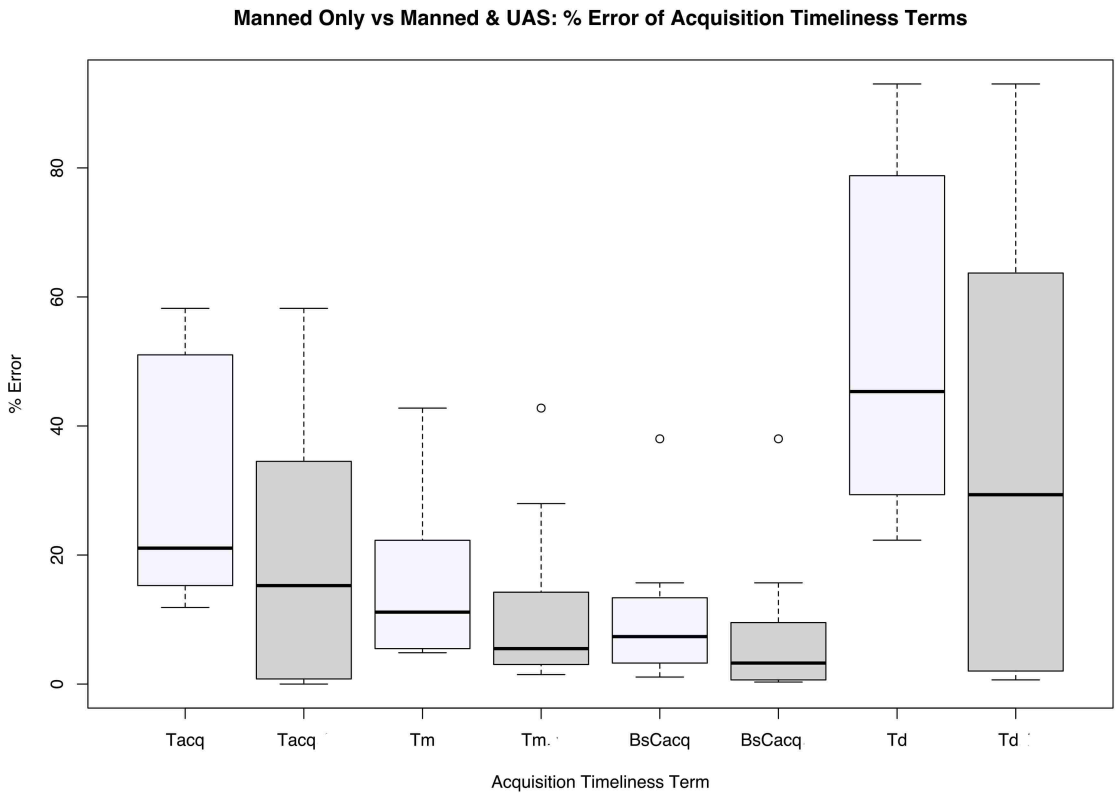

Figure 15: Example of T_M Modeling Source of Error